AGU PUBLICATIONS

Geochemistry, Geophysics, Geosystems

RESEARCH ARTICLE
10.1002/2014GC005534

Key Points:
- The Foulden Maar sediments can be dated to the Oligocene/Miocene boundary
- The magnetic fraction is a population of PSD-sized detrital pyrrhotite
- Magnetic properties indicate a millennial-scale environmental shift

Supporting Information:
- Argon dating methods
- Readme
- Supplementary Figure 1
- Supplementary Data Table 1

Correspondence to:
B. R. S. Fox,
bfox@waikato.ac.nz

Citation:
Fox, B. R. S., J. Wartho, G. S. Wilson, D. E. Lee, F. E. Nelson, and U. Kaulfuss (2015), Long-term evolution of an Oligocene/Miocene maar lake from Otago, New Zealand, *Geochem. Geophys. Geosyst.*, *16*, 59–76, doi:10.1002/2014GC005534.

Received 13 AUG 2014
Accepted 25 NOV 2014
Accepted article online 4 DEC 2014
Published online 9 JAN 2015

Long-term evolution of an Oligocene/Miocene maar lake from Otago, New Zealand

B. R. S. Fox[1], J. Wartho[2], G. S. Wilson[3,4], D. E. Lee[4], F. E. Nelson[3,4], and U. Kaulfuss[4]

[1]School of Science, University of Waikato, Hamilton, New Zealand, [2]School of Earth and Space Exploration, Arizona State University, Tempe, Arizona, USA, [3]Department of Marine Science, University of Otago, Dunedin, New Zealand, [4]Department of Geology, University of Otago, Dunedin, New Zealand

Abstract Foulden Maar is a highly resolved maar lake deposit from the South Island of New Zealand comprising laminated diatomite punctuated by numerous diatomaceous turbidites. Basaltic clasts found in debris flow deposits near the base of the cored sedimentary sequence yielded two new $^{40}Ar/^{39}Ar$ dates of 24.51 ± 0.24 and 23.38 ± 0.24 Ma (2σ). The younger date agrees within error with a previously published $^{40}Ar/^{39}Ar$ date of 23.17 ± 0.19 Ma from a basaltic dyke adjacent to the maar crater. The diatomite is inferred to have been deposited over several tens of thousands of years in the latest Oligocene/earliest Miocene, and may have been coeval with the period of rapid glaciation and subsequent deglaciation of Antarctica known as the Mi-1 event. Sediment magnetic properties and SEM measurements indicate that the magnetic signal is dominated by pseudo-single domain pyrrhotite. The most likely source of detrital pyrrhotite is schist country rock fragments from the inferred tephra ring created by the phreatomagmatic eruption that formed the maar. Variations in magnetic mineral concentration indicate a decrease in erosional input throughout the depositional period, suggesting long-term (tens of thousands of years) environmental change in New Zealand in the latest Oligocene/earliest Miocene.

1. Introduction

Foulden Maar, in the South Island of New Zealand, is a small volcanic crater filled with volcaniclastic debris flows and ~120 m of laminated diatomaceous lake sediments. Previous studies of pollen ages and a single $^{40}Ar/^{39}Ar$ date from a basaltic dyke associated with the maar crater concluded that the deposit is early Miocene in age [*Lindqvist and Lee*, 2009; *Mildenhall et al.*, 2014]. The high (potentially annual) resolution of the lake sediment record combined with the mid-latitude Southern Hemisphere location of New Zealand during the early Miocene [*Sutherland*, 1995] mean that this deposit represents an unrivalled Southern Hemisphere climate archive for a period of often extreme climate variations [e.g., *Miller et al.*, 1991].

Magnetic minerals within sediments can provide valuable information about the prevailing environmental and climatic conditions at the time of deposition [*Thompson and Oldfield*, 1986; *Evans and Heller*, 2003; *Liu et al.*, 2012]. In largely biogenic sediments, the concentration of detrital magnetic minerals can be used as a proxy for the rate of terrigenous input, which in turn provides information about catchment weathering and erosion rates. Magnetic mineralogy can be used to establish the provenance of terrigenous material. However, a major challenge in paleomagnetic studies of sedimentary environments is distinguishing authigenic signatures from detrital [e.g., *Canfield and Berner*, 1987]. In reducing environments, ferrimagnetic iron sulfides such as pyrrhotite can form during diagenesis [*Snowball and Torii*, 1999]. If diagenesis occurs soon after sediment deposition, new magnetic minerals such as greigite may still record the magnetic field at the time of deposition (within a few years) [e.g., *Reynolds et al.*, 1999; *Blanchet et al.*, 2009]. However, doubts have been raised over the possibility that authigenic monoclinic pyrrhotite can form soon after deposition [*Wilkin and Barnes*, 1996; *Horng and Roberts*, 2006]. Many studies have found that apparent magnetic reversals were artifacts introduced by the presence of authigenic pyrrhotite and greigite that formed during later diagenesis [e.g., *Jiang et al.*, 2001; *Weaver et al.*, 2002; *Roberts et al.*, 2010], especially in sediments that have undergone tectonic deformation after deposition. Similarly, authigenic magnetic mineral formation may obscure any climate signal derived from the concentration and mineralogy of the detrital magnetic fraction [e.g., *Blanchet et al.*, 2009].

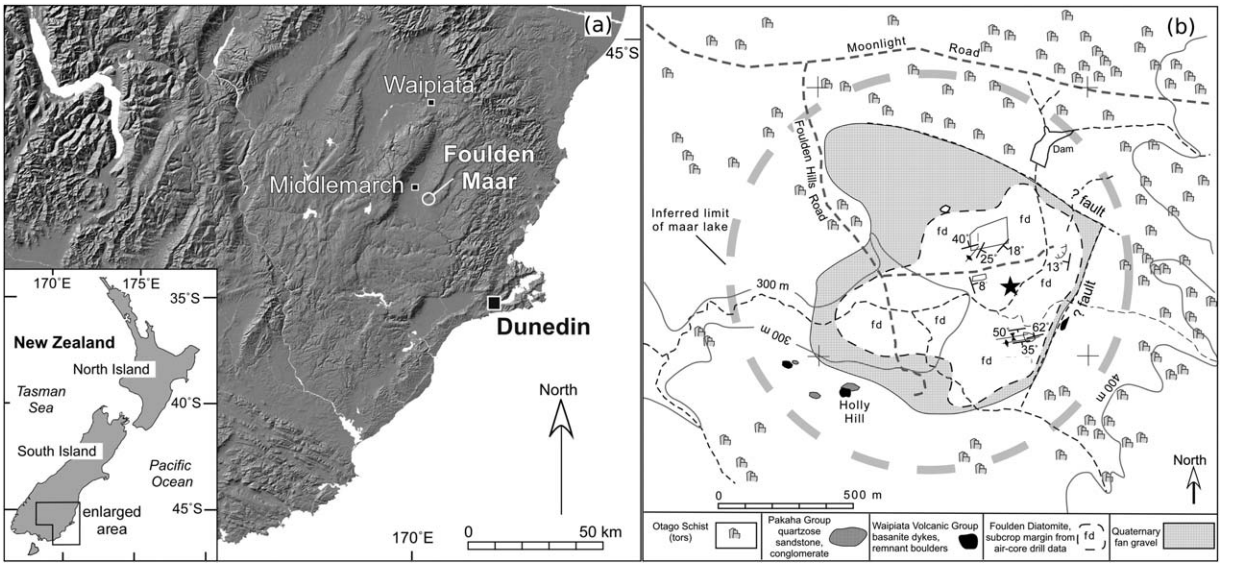

Figure 1. The geological setting of Foulden Maar. (a) Location of Foulden Maar on a map of modern-day New Zealand (reproduced from *Lindqvist and Lee* [2009]); (b) geology of the Foulden Maar area. Drilling location is marked with a star. Modified from *Lindqvist and Lee* [2009].

In this paper, we present two new $^{40}Ar/^{39}Ar$ dates from the base of the Foulden Maar diatomite and use a combination of magnetic measurements and microscopic analysis to investigate the sediment environmental magnetic signal. We infer the presence of detrital pyrrhotite derived from the local country rock, and we use these measurements to infer long-term environmental change in New Zealand in the latest Oligocene/earliest Miocene.

2. Geological Setting

Foulden Maar is a diatomite-filled maar crater located ~45 km northwest of Dunedin, South Island, New Zealand (Figure 1). It forms part of the Waipiata Volcanic Field, which was active during the period 24–9 Ma [*Németh*, 2001; *Coombs et al*., 2008]. The country rock is the Otago Schist, part of the Haast Schist group, which was metamorphosed at latest by the Jurassic and uplifted by the early Cretaceous [*Graham and Mortimer*, 1992; *Adams and Robinson*, 1993]. The schist is cut by the Waipounamu erosion surface, which is dated to the late Cretaceous [*LeMasurier and Landis*, 1996]. Locally, silicified fluvial sandstones and conglomerates are found in the vicinity of the maar [*Lindqvist and Lee*, 2009], but the Cenozoic sediment cover that blankets large areas of Otago [*Forsyth*, 2001] has for the most part been eroded away at this location.

The Otago Schist in the region of Foulden Maar comprises both greenschist and greyschist facies. Although the majority of the schist in this area is greyschist, small areas of greenschist crop out close to the maar crater [*Forsyth*, 2001]. The greenschist in the region contains minor magnetite, pyrite, and pyrrhotite while the greyschist contains minor pyrite and pyrrhotite [*Craw*, 1984; *Hay and Craw*, 1993].

The maar crater is approximately 800 m in diameter (Figure 1b), although erosion estimates suggest that it may originally have been 1.5 km wide [*Németh*, 2001]. The crater walls dip at an angle of 82°. Two drill cores retrieved in 2009 (FH1 and FH2) comprise ~120 m of laminated diatomite underlain by ~60 m of allochthonous sands, muds, and breccias, mostly composed of country rock and volcaniclastic material (Figure 2).

3. Sampling and Methods

3.1. Sediment Characteristics and Composite Depth Scale

Of the two cores, FH2 had the highest recovery (>95%). We used this core for all analyses reported in this paper. However, in intervals where FH2 was damaged or incomplete, we spliced in sections of FH1 where these were better preserved. We used visual correlation of turbidites and individual laminae to splice

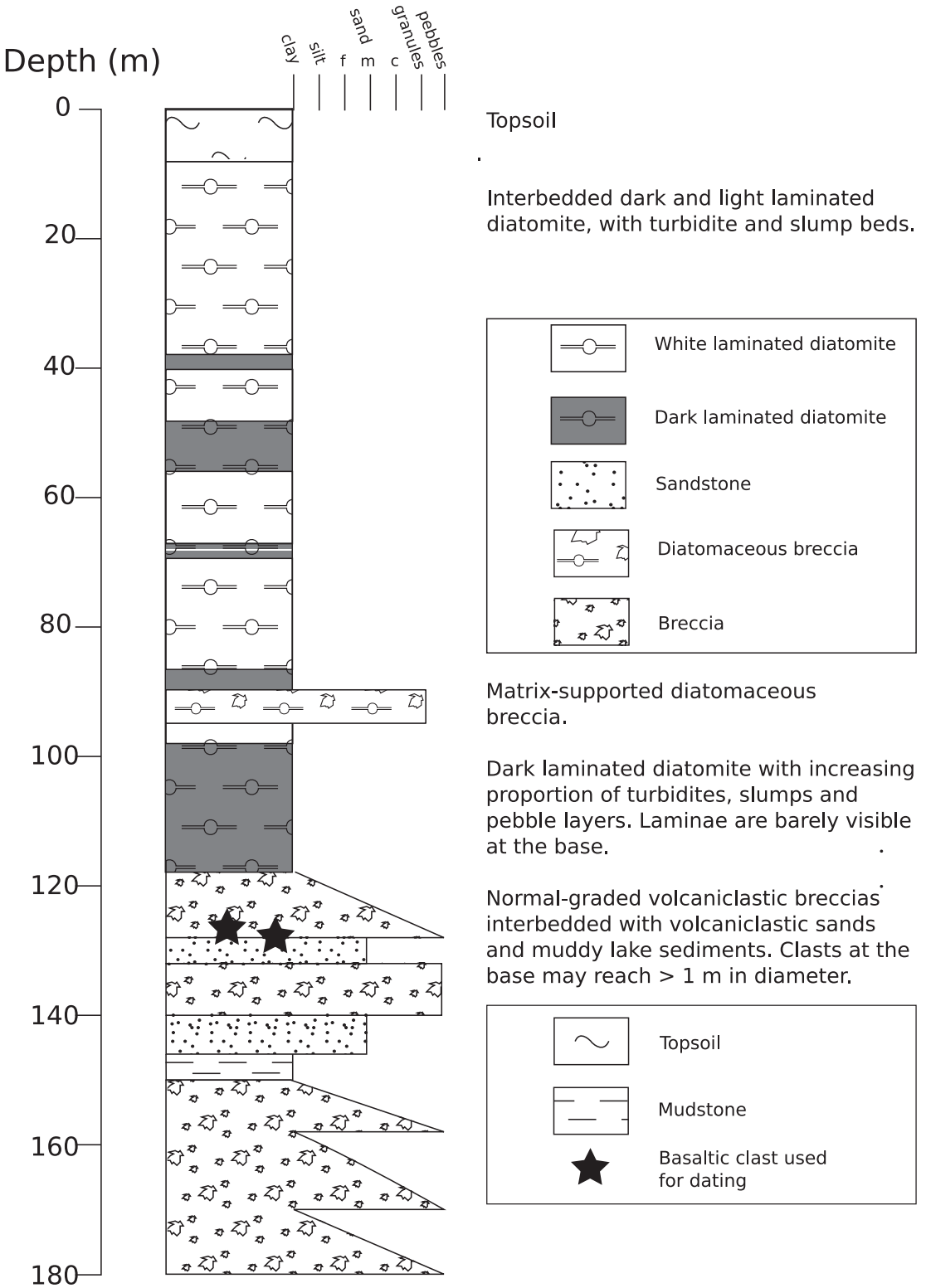

Figure 2. Graphic log of FH2, the longer of the two cores retrieved from Foulden Maar for this study, indicating the depths from which the $^{40}Ar/^{39}Ar$ dates were obtained.

sections of FH1 into FH2. We constructed a composite depth-scale based on this spliced section. Composite depths are reported here as meters composite depth (mcd), while depths below surface in core FH2 are reported as meters (m).

In order to define some basic characteristics of the Foulden Maar diatomite, we performed a basic facies analysis and measured the thickness of all event beds (turbidites, slumps, and breccia intervals). We also measured the thickness of light/dark couplets in several representative intervals downcore. We made these couplet measurements using high-resolution (20 pixels/mm) digital photographs taken using a Geotek Multi-Sensor Core Logger equipped with a line-scan camera.

3.2. $^{40}Ar/^{39}Ar$ Dating

$^{40}Ar/^{39}Ar$ measurements were obtained from two basaltic clasts, V14 and V15, found at depths of 126.30 and 126.80 m, respectively, in core FH2. Both clasts were obtained from a coarse-grained gravity flow horizon that is interpreted as having originated at the tephra rim of the maar during the earliest phase of lake sediment deposition. Both clasts had a thin alteration rim that was removed before sampling. Whole-rock measurements were used, as the basalts were too fine grained to allow mineral picking of individual K-bearing grains.

$^{40}Ar/^{39}Ar$ measurements of the two basalt samples were undertaken at the Noble Gas Laboratory at Rutgers University, following methods similar to those described by *Turrin et al*. [1994, 1998, 2008, 2010]. $^{40}Ar/^{39}Ar$ measurements of the age standards and salts were undertaken at the Noble Gas Geochemistry and Geochronology Laboratories at Arizona State University. For a more detailed description of the $^{40}Ar/^{39}Ar$ dating method, see supporting information.

3.3. Magnetic Methods

Following initial low-resolution physical properties logging, the drill core was split longitudinally using a diamond-bladed circular saw. Samples were taken from the split face of the diatomite section. All samples discussed in this study were taken using non-magnetic materials. Cube samples were cut using 6 cm^3 plastic sample boxes and a ceramic knife. Powdered samples were crushed using a quartz mortar and pestle. U-channel samples [*Weeks et al*., 1993] were taken by pushing the u-channel into the split face of the core and running nylon fishing line through the core behind the u-channel to free the sample from the surrounding sediment. U-channel samples were taken from 6 to 106 m, with the exception of the coarse-grained diatomaceous breccias at $\sim$95 m.

We simultaneously measured the low-field volume magnetic susceptibility (κ) and gamma attenuation density at 0.5 cm intervals using a Geotek Multi-Sensor Core Logger equipped with a Bartington Instruments MS2E point sensor. The point sensor was zeroed at 10 cm intervals. We calibrated the κ data using whole-core measurements taken at 2 cm stratigraphic intervals with a Bartington Instruments MS2C loop sensor with 10 cm diameter. The loop was factory calibrated by Bartington Instruments and checked over the long term by a Geotek technician using a calibration sample provided by the manufacturers. In all cases, cores were allowed to warm to room temperature before measurement, and ambient temperature was monitored throughout the measurement process to detect unacceptable drift ($>5^{\circ}$C). Temperatures were found to vary by $<1^{\circ}$C within a given measurement session, and by 3.6°C over all sessions. We consider this to be an acceptable level of drift that is unlikely to affect the robustness of results.

With the exception of κ measurements, which we found to be reproducible, all other in-field measurements of the diatomite (such as hysteresis loops and temperature dependence of magnetic susceptibility) failed to produce robust results. All such measurements produced noisy results. This is probably due to the low concentrations of magnetic material in the sediment, combined with the high concentrations of diamagnetic silica. We restricted the rest of our magnetic investigation to remanence-based measurements. Natural remanent magnetization (NRM) was stable throughout the core; these results will be presented elsewhere.

An anhysteretic remanent magnetization (ARM) was imparted to u-channel samples, which were then measured and demagnetized using a 2-G Enterprises cryogenic magnetometer [*Weeks et al*., 1993] housed in a low-field (150 nT) room at the Otago Palaeomagnetic Research Facility (OPRF). U-channels were first placed in the low-field room for 24 h to allow relaxation of viscous magnetizations. An ARM was then imparted in a DC bias field of 0.063 mT and an alternating field (AF) of 100 mT. This ARM was then subjected to AF demagnetization in increments of 6 mT to 60 mT, and then at 75, 90, 105, and 120 mT. We measured the ARM at 1 cm stratigraphic intervals through the core from depths of 6 to 106 m, with the exception of the diatomaceous breccia interval at $\sim$95 m.

Isothermal remanent magnetization (IRM) acquisition curves were generated by subjecting discrete samples to progressively increasing DC fields up to 1 T. IRMs were imparted using an ASC Scientific IM-10 impulse

magnetizer and measured and subsequently demagnetized using a 2-G Enterprises cryogenic magnetometer. We measured a total of 22 samples from throughout the diatomite succession.

IRM acquisition curves are generally assumed to represent a linear addition of the weighted sum of remanence of each magnetic component within the assemblage [*Heslop and Dillon*, 2007]. In the case of an assemblage where several components make significant contributions to the overall remanence, as is common in sedimentary deposits, the parameters of the overall curve will not enable identification of any given component within the assemblage. IRM acquisition curves can be "unmixed," or decomposed into the contributions of individual components, using statistical modeling [e.g., *Robertson and France*, 1994; *Kruiver et al*., 2001; *Heslop et al*., 2002; *Egli*, 2003; *Heslop and Dillon*, 2007]. However, statistical tests for calculating the optimal number of components often result in an overly complex model [*Heslop et al*., 2001].

In order to reduce noise in the IRM acquisition curve, we first averaged curves for 3–4 samples. We then used the software described by *Heslop et al*. [2002] to estimate the number of components. As a check on the model, we created "virtual" IRM acquisition curves from the cumulative log-Gaussian (CLG) curves using the approach outlined by *Lurcock* [2012] and compared them to known magnetic mineral behavior.

A three-component IRM [*Lowrie*, 1990; *Torii et al*., 1996] was imparted to 34 samples of diatomite and 5 samples of schist derived from a country-rock boulder found at the base of the cored succession. IRMs were imparted in orthogonal directions at 1, 0.4, and 0.12 T. The samples were then stepwise thermally demagnetized using a magnetically shielded oven equipped with an ASC Scientific TD-48SC Thermal Specimen Demagnetizer at temperatures up to 680°C. Samples were held at each peak temperature for 20–30 min and were then fan cooled at a rate of 10–35°C/min. After each heating/cooling cycle, we measured the κ and remanence of the samples using a Bartington Instruments magnetic susceptibility meter and a 2-G Enterprises cryogenic magnetometer.

3.4. SEM Measurements

We studied representative polished sediment samples using a Zeiss Sigma VP FEG scanning electron microscope (SEM) operated at 15 kV at the Otago Centre for Electron Microscopy (OCEM). We performed energy-dispersive X-ray spectra (EDS) elemental analyses of selected mineral grains using a HKL INCA Premium Synergy Integrated EDS/EBSD system. We used polished samples of pyrrhotite and pyrite to calibrate the EDS system for atomic ratios of iron to sulfur.

4. Results

4.1. Core Description

The laminated diatomite consists of ~95,000 light-dark couplets ranging in thickness from <0.5 to 2 mm (Figures 3a–3b). It can be divided into two major facies on the basis of color: white laminated diatomite (WLDA), comprising 41% of the entire succession (Figure 3a) and dark laminated diatomite (DLDA), comprising 9% of the succession (Figure 3b). Both laminated facies are characterized by alternating light and dark laminae, here termed light-dark couplets. Couplet thickness variation is largely determined by the thickness of the light layer (standard deviation 0.14 mm for those sections studied), with the dark layer relatively invariant (standard deviation 0.05 mm). In general, average couplet thickness decreases downcore, from an average of 0.52 mm in the top 10 m to 0.46 mm near the base. Average couplet thickness is higher in white laminated diatomite (average 0.5 mm) than in dark laminated diatomite (average 0.3 mm).

Both laminated diatomite facies are composed almost entirely (>98%) of frustules of the diatom *Encyonema jordanii* and organic carbon. Total organic carbon in WLDA averages ~6%, while in DLDA it averages ~12%. The remainder of the sediment is composed of sponge spicules and chrysophycean cysts. The abiogenic component throughout most of the laminated diatomite facies is so minor as to be undetectable by macro or conventional microscopic investigation, although magnetic remanence measurements and SEM observations indicate the presence of detrital magnetic grains (see below). However, framboidal authigenic pyrite is visible in some horizons.

The laminated succession is interrupted by >1000 diatomaceous turbidites that range in thickness from <1 cm to almost 1 m (Figure 3d). These turbidites comprise 41% of the entire succession. Turbidites from the uppermost section of the deposit are described in detail in *Lindqvist and Lee* [2009] (there called

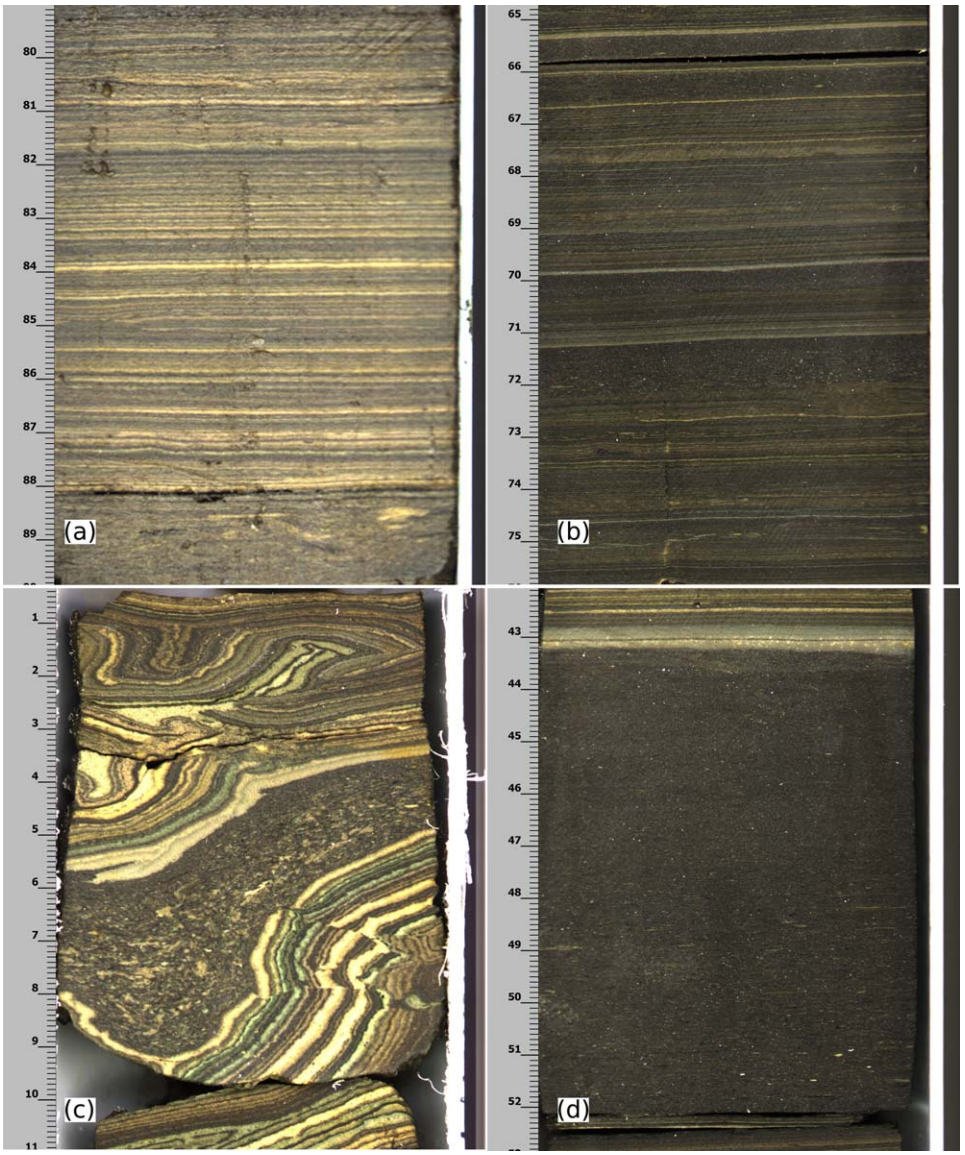

Figure 3. The major diatomite facies found in FH2. (a) White laminated diatomite (11 m); (b) dark laminated diatomite (38 m); (c) slumped diatomite (69 m); (d) diatomaceous turbidite with fine-grained, pale-colored capping layer (38 m). Scales to the left of each image are in centimeters.

"speckled beds"). They are composed largely of similar materials to the WLDA and DLDA facies, but with an increased proportion of organic matter (averaging 8%) and detrital material. Detrital material ranges from quartzose silt to schist and basalt pebbles, and is generally found at the base of the turbidites, where it may form layers up to 1 cm thick. Sand-sized grains were found by *Lindqvist and Lee* [2009] to be schistose in nature. The detrital component is interpreted to be derived from the surrounding schist country rock and from the products of the original maar-forming eruption. Turbidites in the succession are overlain by a thin ($<$1 mm–2 cm) white, gray, or yellow capping layer. This capping layer is largely composed of diatoms, but also includes a clay mineral component. The capping layers often have high κ compared with the surrounding sediment. This is interpreted as due to the clay mineral content.

Below $\sim$40 m, the laminated diatomite is also interbedded with centimeter to decimeter-scale slumped beds (Figure 3c), which make up 9% of the succession and increase in frequency and thickness downcore. They range from slightly deformed intervals where individual laminae are still clearly visible to strongly deformed intervals where lamina boundaries can no longer be distinguished. Slumped intervals may also include deformed turbidites.

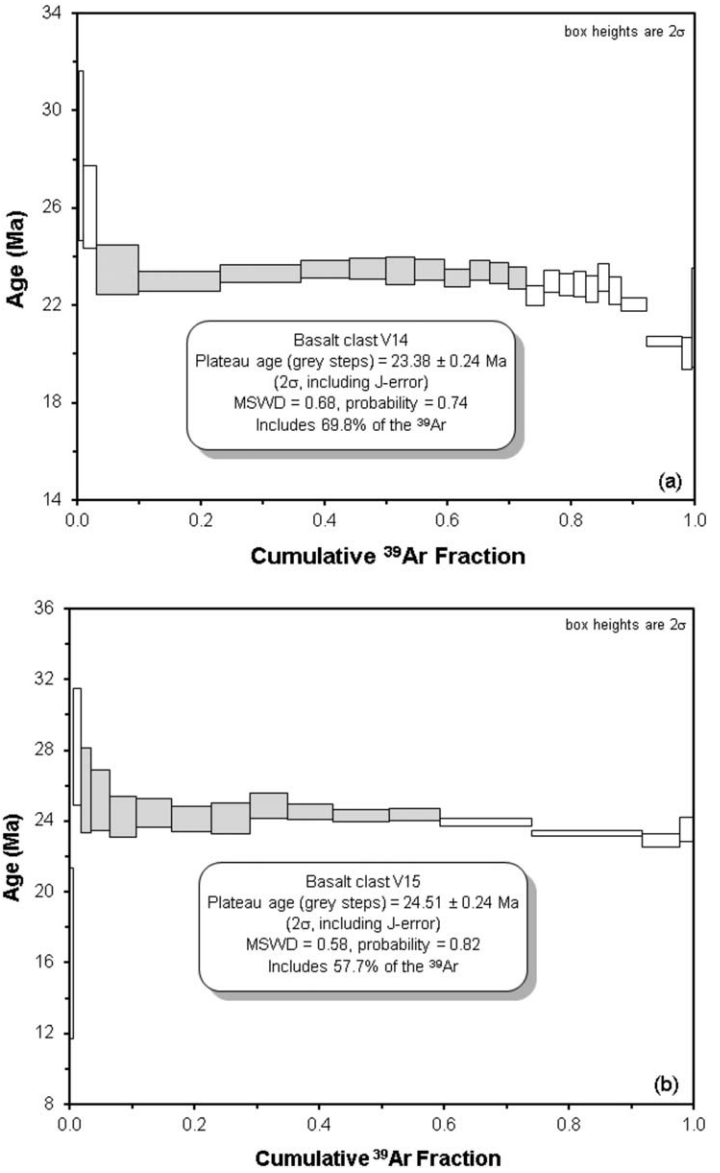

Figure 4. $^{40}Ar/^{39}Ar$ plateau ages for basalt samples from Foulden Maar. (a) Sample V14; (b) sample V15.

Two major allochthonous intervals occur in the laminated diatomite succession, at ~68 and 89–94 m depth. These include coarse-grained breccias containing pebbles of schist and vesicular basalt, which often have altered rims. We interpret the detrital schist and basalt components as fragments of country tock and products of the maar-forming eruption.

4.2. $^{40}Ar/^{39}Ar$ Dates

^{39}Ar age spectra for samples V14 and V15 are shown in Figure 4. Ca/K ratios are 0.0–39.7 and 0.0–23.37 for samples V14 and V15, respectively, which are normal for whole-rock basalts. High-Ca/K ratios probably signify degassing of plagioclase grains. The plateau age of sample V14 is 23.38 ± 0.24 Ma (2σ) for 69.8% of the released ^{39}Ar (Figure 4a), and also gives an inverse isochron (from the plateau age steps) of 23.45 ± 0.31 Ma (95% conf., mean square of weighted deviation (MSWD) = 0.67), yielding a $^{40}Ar/^{36}Ar$ ratio of 295.1 ± 1.5, which is within error of the $^{40}Ar/^{36}Ar$ atmospheric ratio of 295.5 [*Steiger and Jäger*, 1977]. The plateau age of sample V15 is older at 24.51 ± 0.24 (2σ) for 57.7% ^{39}Ar release (Figure 4b), with a similar inverse isochron (from the plateau age steps) of 24.43 ± 0.30 Ma (95% conf., MSWD = 0.55), and a $^{40}Ar/^{36}Ar$ ratio of 295.9 ± 0.9. Both samples show evidence of disturbed low-temperature ages and variable Ca/K ratios, which is common in $^{40}Ar/^{39}Ar$ whole-rock basalt samples. In addition, atmospheric ^{40}Ar values are variable in the steps for both samples, i.e., 5.2–94.5% in sample V14, but are higher (17.9–96.5%) in sample V15. High atmospheric ^{40}Ar values possibly indicate a high degree of alteration of basalt samples.

4.3. Alternating-Field Demagnetization of ARM

Normalized ARM demagnetization curves are plotted in Figure 5 against reference curves from *Peters and Thompson* [1998]. Each curve represents an average of 20 measurements over a 2 m interval, covering the diatomite succession between 6 and 106 m depth in FH2. The curves are similar in shape throughout the succession, which suggests no major variation in magnetic mineral assemblage with depth. Many of the curves fall within the magnetite field (Figure 5a). However, up to 30% fall outside this field for the 40–80 mT demagnetization interval. The fact that all curves fall well within the pyrrhotite field is not highly informative, given that this field covers almost the entire plot (Figure 5b). The fact that all the data fall outside the greigite field indicates that greigite can be ruled out as the principal magnetic mineral (Figure 5c).

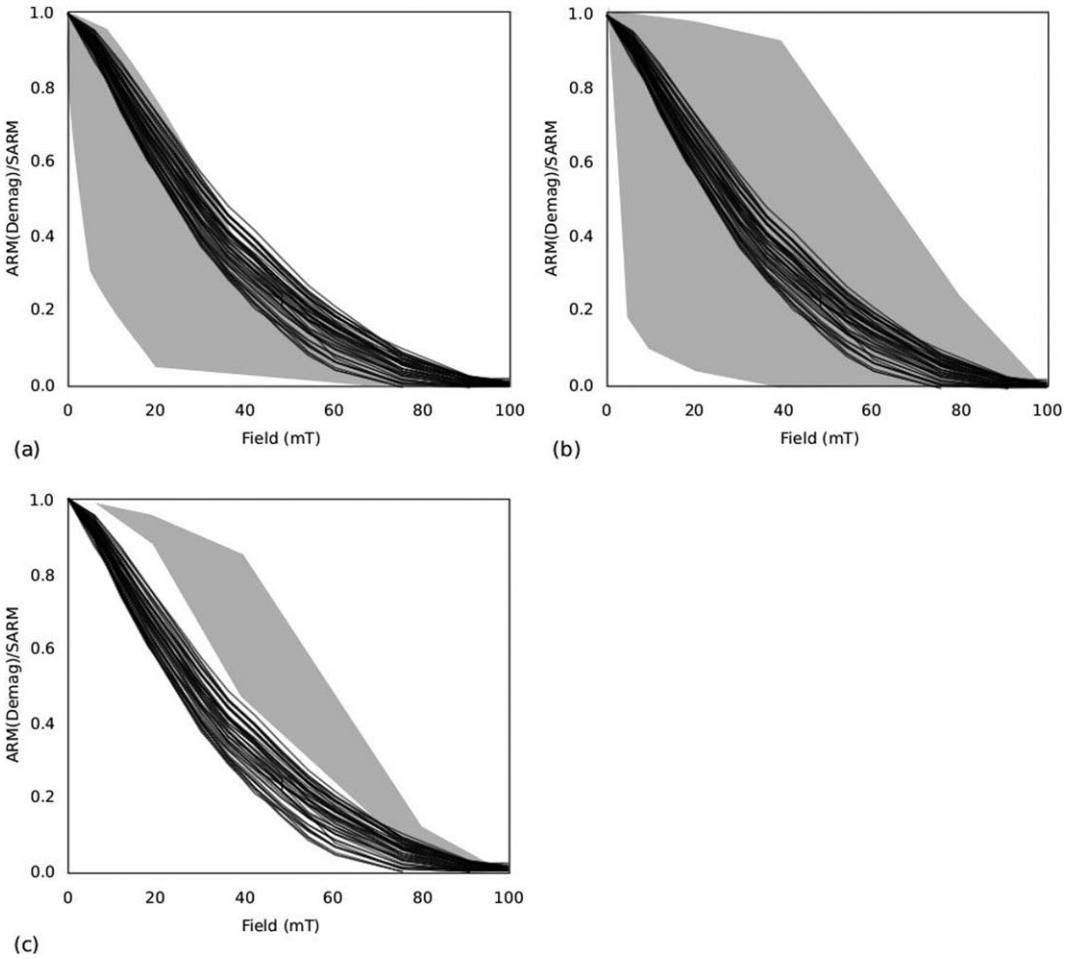

Figure 5. Normalized average ARM demagnetization curves for the Foulden Maar core (black lines) plotted against the range of reference curves (shaded) for (a) magnetite, (b) pyrrhotite, and (c) greigite (redrawn from *Peters and Thompson* [1998]). SARM = saturation ARM.

4.4. IRM

All IRM acquisition curves for samples from the Foulden Maar diatomite are similar in shape, regardless of their depth in the core. The only major difference is the IRM intensity, which reflects the concentration of ferrimagnetic minerals. A comparison of IRM acquisition curves with reference curves for magnetite and pyrrhotite, respectively [*Symons and Cioppa*, 2000], is shown in Figures 6a and 6b. Reference curves for hematite and goethite are sufficiently different from our measurements that we do not reproduce them here. From this comparison, pyrrhotite is the most likely primary remanence carrier in the studied sediments (Figure 6b). A similar comparison with the reference curves of *Peters and Thompson* [1998] (Figures 6c–6e) again indicates that pyrrhotite is the most likely candidate (Figure 6e), with magnetite also possible (Figure 6c). A comparison with reference curves for greigite from *Peters and Thompson* [1998] (Figure 6d) and *Roberts et al*. [2011] (Figure 6f) indicates that greigite is unlikely to be the principal remanence carrier.

A second approach used by *Symons and Cioppa* [2000] was to plot the "crossover point" where the IRM acquisition curve crosses the AF demagnetization curve for saturation IRM (SIRM), which is defined here following *Symons and Cioppa* [2000] as the IRM acquired in a DC field of 900 mT. These points are shown on a reference plot for pyrrhotite and magnetite [*Symons and Cioppa*, 2000] in Figure 7. Although one point falls within both the pyrrhotite and magnetite domains, the rest fall outside the magnetite domain and within the domains for PSD and SD pyrrhotite.

In all cases, CLG unmixing of averaged acquisition curves predicted two components that contribute approximately equally to the total IRM [*Heslop et al*., 2001]. Each component, when reconstructed, fits the

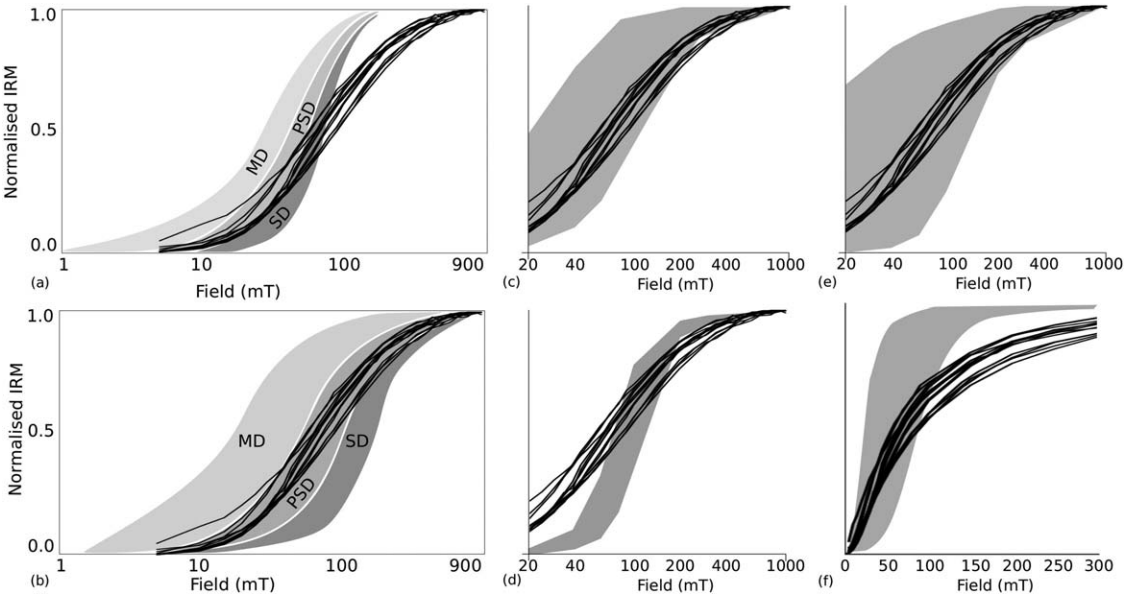

Figure 6. IRM acquisition curves from the Foulden Maar diatomite compared with reference curves from *Symons and Cioppa* [2000] for single domain (SD), pseudo-single domain (PSD), and multidomain (MD) populations of (a) magnetite and (b) pyrrhotite; with reference curves from *Peters and Thompson* [1998] for (c) magnetite, (d) greigite, and (e) pyrrhotite; and with a range of reference values from *Roberts et al.* [2011] for (f) greigite. Black lines represent Foulden Maar data and shaded areas represent reference curves.

reference curve for pyrrhotite most closely. However, neither component fits the pyrrhotite reference curve as closely as do the original acquisition curves. If we take the models at face value, they indicate that the mineralogy is a mixture of two populations of pyrrhotite with different coercivity characteristics. However, the data were noisy and the model fit to the IRM curves was poor in most cases. In several cases, unmixing of a single IRM acquisition curve produced a one-component model, while unmixing of an average of 3–4 curves produced a two-component model. This, combined with the reduction in goodness of fit to the magnetic mineral reference data after unmixing, suggests that the statistical model may have overestimated the complexity of the mineralogy due to the noisy nature of the data [*Heslop et al.*, 2001]. The reconstructed curves compared with reference curves from *Symons and Cioppa* [2000] are shown in supporting information Figure 1.

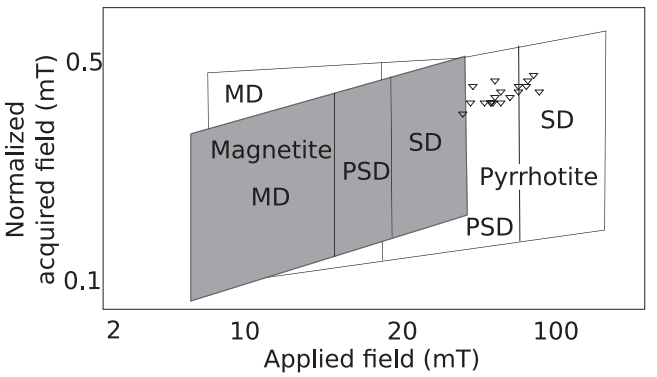

Figure 7. Crossover points for IRM acquisition and AF demagnetization curves of SIRM for the Foulden Maar data, plotted against a reference plot for magnetite and pyrrhotite (redrawn from *Symons and Cioppa* [2000]). The applied field in mT (DC for IRM acquisition, AF for IRM demagnetization) is represented on the *x* axis, while the magnetization of the sample as a fraction of the IRM acquired in a field of 900 mT is represented on the *y* axis. The triangles mark the points where acquisition and demagnetization curves for a given sample intersect.

4.4.1. IRM Parameters

Along with the shape of IRM acquisition and demagnetization curves, a number of other IRM parameters can also be used to help define magnetic mineralogy. The coercivity of remanence (H_{cr}) is the magnitude of the backfield required to reduce the magnetic moment of a sample from saturation to zero. The remanent acquisition coercive force (H'_{cr}) is the field required for the sample to acquire half of its SIRM. Reference ranges of H_{cr}, H'_{cr}, and H_{cr}/H'_{cr} are given by *Peters and Dekkers* [2003]. In Figure 8a, these ranges are visually compared with the Foulden Maar data. The upper and lower limits of each range are plotted in a graph of H_{cr}

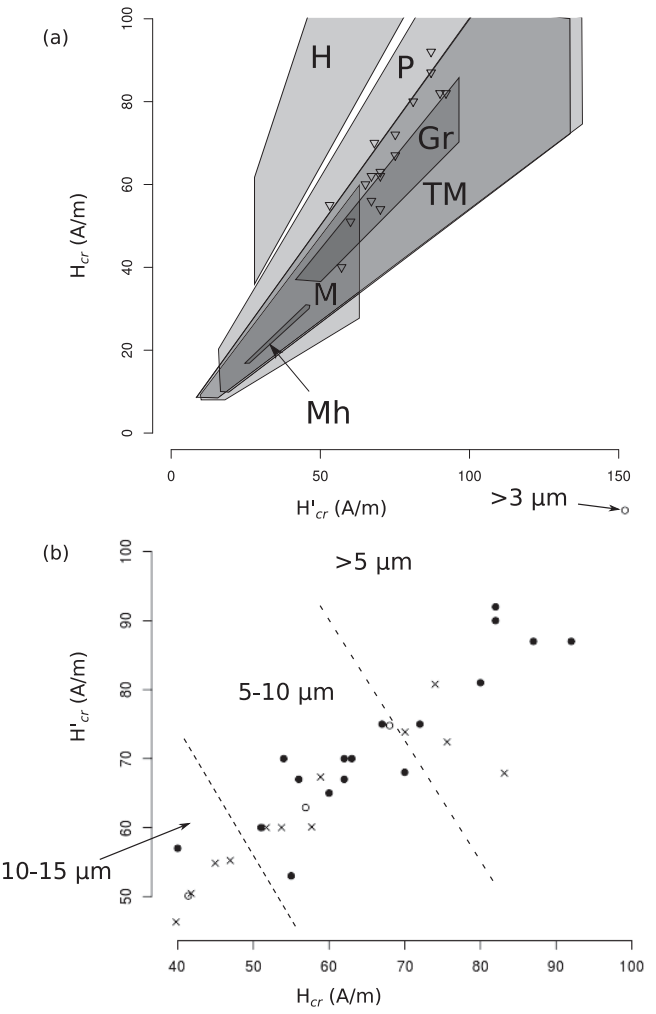

Figure 8. H'_{cr} and H_{cr} values for the Foulden Maar samples compared with reference data. (a) H'_{cr} and H_{cr} region for each mineral discussed by *Peters and Dekkers* [2003], with Foulden Maar data plotted as inverted triangles. M = magnetite, TM = titanomagnetite, Mh = maghemite, H = hematite, P = pyrrhotite, Gr = greigite. Goethite is not plotted because all values are beyond the area of the graph. (b) H_{cr} versus H'_{cr} for the Foulden Maar data (solid circles) plotted with the data for sized fractions of pyrrhotite given by *Dekkers* [1988] (crosses) and *Clark* [1984] (empty circles).

versus H'_{cr}. This provides a polygon of up to six sides for each mineral. Many H_{cr} and H'_{cr} values for the Foulden Maar samples fall into several overlapping regions. However, the only region that contains all of the data is that for pyrrhotite. The main alternative contender is titanomagnetite, which also has variable magnetic properties that span much of the parameter space in Figure 8a. However, some of the data points fall outside the titanomagnetite field.

Given that most of our results indicate a pyrrhotite component in the Foulden Maar assemblage, it is worth comparing the coercivity parameters to reference data for sized pyrrhotite fractions [*Clark*, 1984; *Dekkers*, 1988] (Figure 8b). The Foulden Maar data have approximately the same trend as the reference grain-size trend, and mostly fall into the 3–10 μm range. This fits well with the evidence discussed above for PSD to SD properties in the Foulden Maar samples; the PSD size range for pyrrhotite is 2–40 μm, while the SD size range is 0.017–2 μm [*Clark*, 1984; *Dekkers*, 1988].

4.4.2. Thermal Demagnetization of a Three-Component IRM

Thermal demagnetization measurements of the diatomite resulted in combustion of organic matter at ~200–250°C. This led to alteration of the magnetic mineral assemblage. Above ~50 m depth, this alteration resulted in a complete loss of remanence (Figure 9a). Below this depth, 15–20% of the initial remanence remained, and the samples were not fully demagnetized until ~680°C, which suggests the presence of a minor hematite component (Figure 9b). Unfortunately, due to the alteration of the mineral assemblage at relatively low temperatures, the main magnetic carrier cannot be identified from these measurements.

The schist samples underwent a steep decline in remanence at 330–360°C (Figure 9c). In one sample, this decline did not reach zero, and the remaining remanence declined to zero in the range 550–680°C (Figure 9d). These results indicate the presence of impure pyrrhotite (Curie temperature 325°C, potentially rising with impurities [*Vaughan et al*., 1971]) with minor hematite (Curie temperature 680°C).

4.5. Downcore Magnetic Susceptibility and ARM Variations

Magnetic susceptibility (κ) and ARM records for the Foulden Maar diatomite are shown in Figure 10. Both ARM and κ values are generally low. However, several patterns can be observed in both records. ARM and κ both increase downcore with similar patterns of variation (Figure 10). ARM and κ can both be thought of as

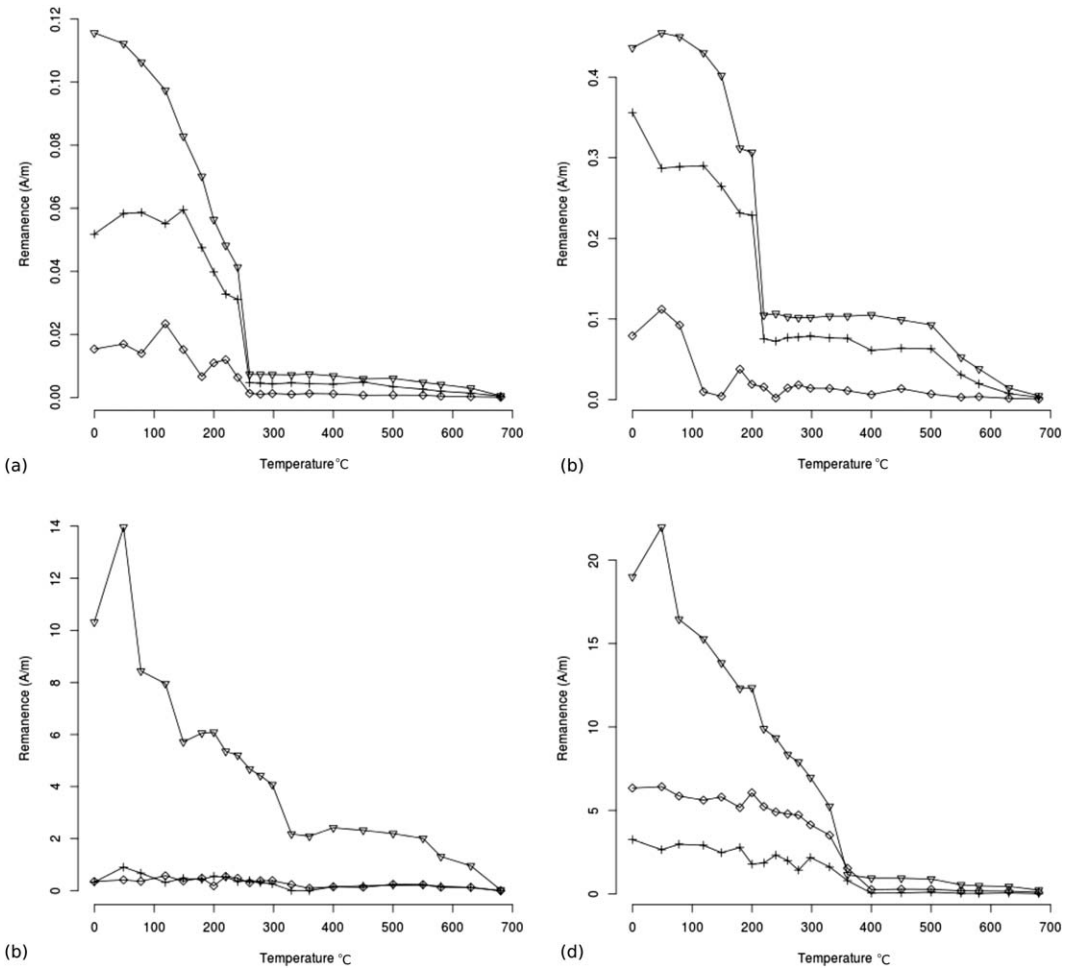

Figure 9. Stepwise thermal demagnetization curves for a three-component IRM for selected samples from Foulden Maar. IRM was imparted in three orthogonal directions at 0.12 (▽), 0.4 (+), and 1 T (◇). Samples are from (a) 10.65 m and (b) 63.80 m; (c and d) samples from a schist boulder found in the diatreme breccia at ∼183 m. The sample shown in Figure 9c undergoes major unblocking between 300 and 330°C; that shown in Figure 9d undergoes major unblocking between 330 and 360°C.

measures of magnetic mineral concentration. Although both can be affected by other factors—concentration of paramagnetic minerals for κ and magnetic mineral assemblage for both—covariance of the two measures, combined with other indications of a homogeneous magnetic mineral assemblage downcore, suggest that these measurements primarily record concentration variations. The ARM and κ records can be divided into two zones. Zone A, from the base of the diatomite succession to ∼39 mcd, has relatively high and variable ARM and κ values (ARM mean 7.56×10^{-4} A/m, $\sigma = 1.00 \times 10^{-3}$ A/m, κ mean 0.92×10^{-5} SI, $\sigma = 1.5 \times 10^{-5}$ SI). Zone B, from ∼39 mcd to the top of the deposit, has low κ values and relatively low variability (ARM mean 2.06×10^{-4} A/m, $\sigma = 1.22 \times 10^{-4}$ A/m, κ mean -0.34×10^{-5} SI, $\sigma = 0.5 \times 10^{-5}$ SI; Figure 10). IRM, ARM and κ also vary with facies. For all three parameters, values are highest in turbidite intervals and lowest in WLDA intervals, with DLDA intervals having intermediate values.

4.6. SEM Observations

Although the concentration of terrigenous material in the sediment samples was low, we identified a number of pyrrhotite grains in the size range 1–2 μm. These grains are broken or fragmented, but may originally have been hexagonal (Figures 11a and 11b). EDS spectra (Figures 11c and 11d) have iron:sulfur ratios that range from 0.86 to 1.01 for these grains, which indicates the presence of both monoclinic (ferrimagnetic) and hexagonal (antiferromagnetic) pyrrhotite. We also identified 1–2 μm sized particles of a number of other metals, including native copper and native iron. The copper particles were by far the most abundant (although still low in absolute concentration), and had extensive surface damage (Figures 11e and 11f).

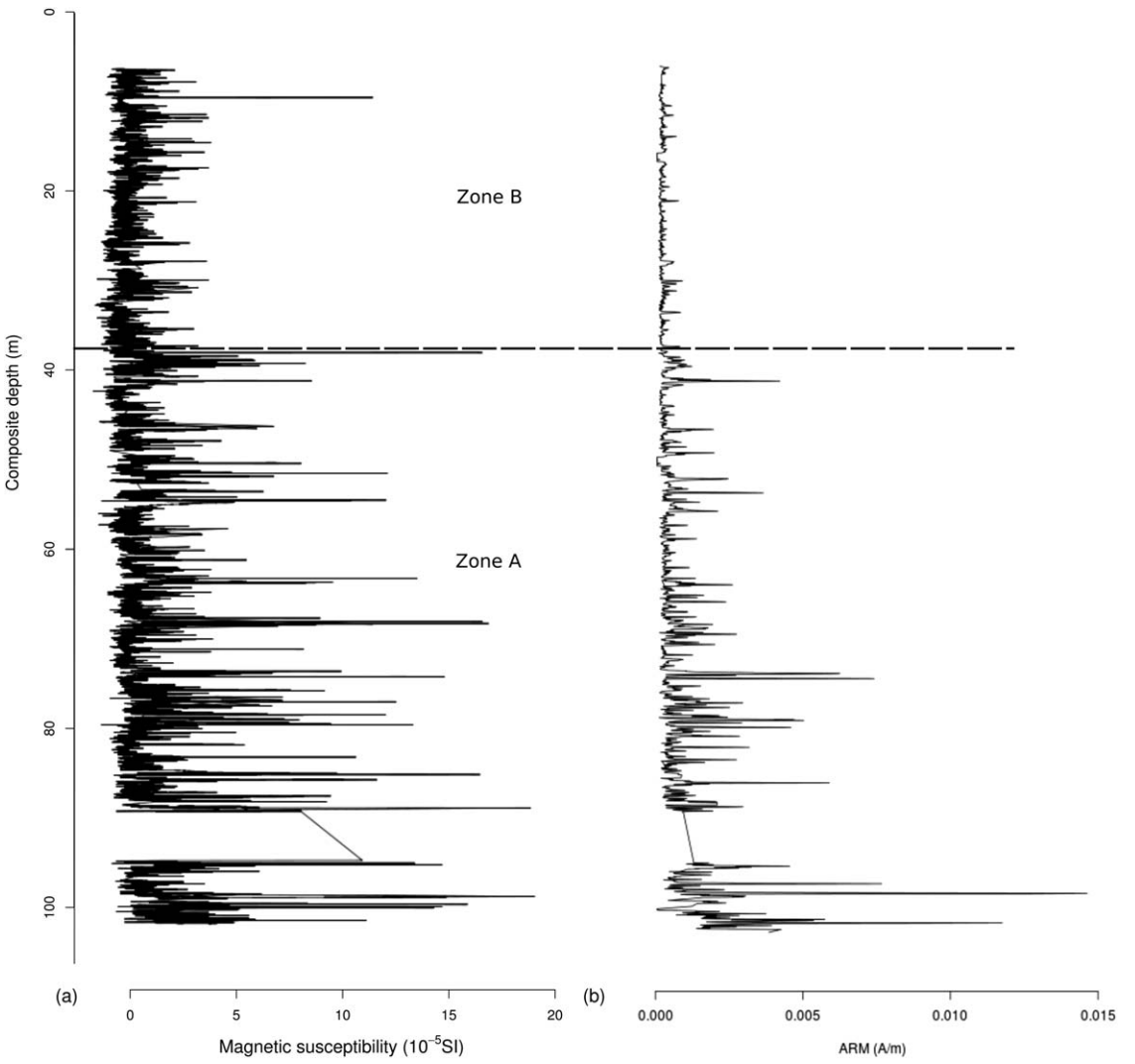

Figure 10. Magnetic susceptibility (κ) and ARM variations for the laminated diatomite interval of the Foulden Maar core. Magnetic behavior zones are marked (see text for discussion). The gap at ~90 m represents a section of volcaniclastic breccias with high κ (see Figure 2).

These metal and sulfide grains are isolated and well dispersed through the sediment, and do not occur in association with each other or in obvious veins or intergrown masses. We also observed a number of iron sulfide grains with similar composition to pyrrhotite (iron:sulfur ratios 0.77–0.99) in a schist sample from a country rock boulder at the base of the core. No magnetite or titanomagnetite grains were observed by SEM in either the diatomite or the schist.

5. Discussion

5.1. $^{40}Ar/^{39}Ar$ Dating of the Foulden Maar Diatomite

Different basalt $^{40}Ar/^{39}Ar$ ages from the Foulden Maar deposit (23.38 ± 0.24 Ma for V14 and 24.51 ± 0.24 Ma (2σ) for V15) indicate that the clasts used for dating are unlikely to be sourced from a single eruption. Sample V15, at least, must be from an eruption that predated the formation of the maar (a nearby eruption has been dated to 24.8 ± 0.6 Ma [*Hoernle et al*., 2006]). This inference is supported by the proportion of atmospheric ^{40}Ar contained in V15, which is higher (17.9–96.5% atmospheric ^{40}Ar) than in sample V14 (5.2–94.5% atmospheric ^{40}Ar), and indicates a greater degree of chemical alteration. However, given that both clasts occur in gravity flow deposits, it is likely that both are reworked, and without further information they provide only a maximum age for the lake sediments of 23.38 ± 0.24 Ma (2σ).

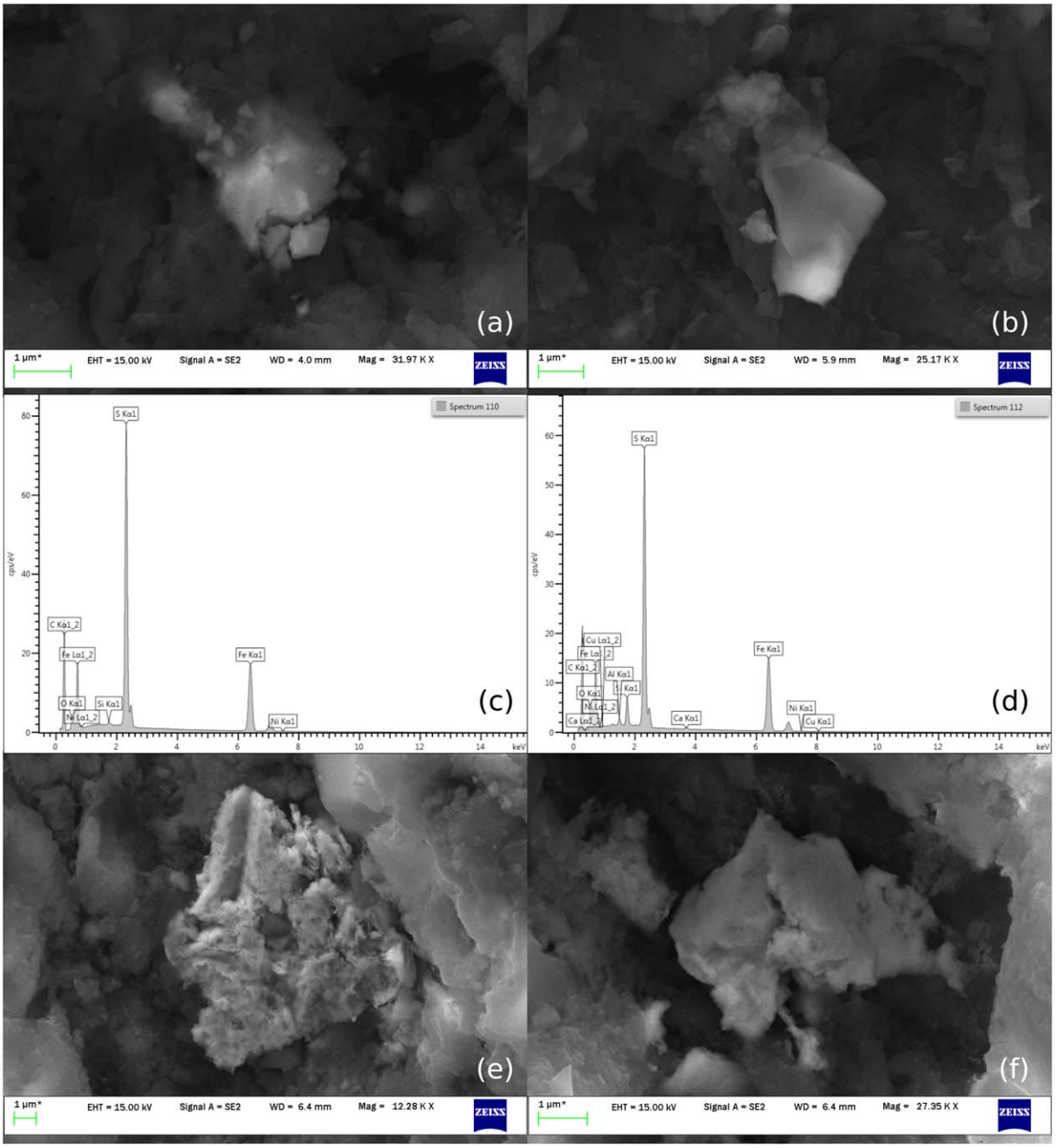

Figure 11. SEM images of grains from the Foulden Maar sediment. (a) Monoclinic pyrrhotite grain, Fe:S ratio = 0.86. (b) Hexagonal pyrrhotite grain, Fe:S ratio = 1:01. (c) EDS spectrum for grain shown in Figure 11a. (d) EDS spectrum for grain shown in Figure 11b. (e and f) Native copper (Cu = ~80 atomic %).

A single $^{40}Ar/^{39}Ar$ date of 23.17 ± 0.19 Ma had previously been obtained from a basaltic dyke at Holly Hill, ~50 m from the edge of the Foulden Maar crater [*Lindqvist and Lee*, 2009], and represents the age of maar formation. The Holly Hill date of 23.17 ± 0.19 Ma and the Foulden Maar date of 23.38 ± 0.24 (2σ) agree within error. Sample V14 may, therefore, derive from the same eruptions that formed the maar and the Holly Hill dyke. The presence of late Oligocene to early Miocene (late Waitakian to early Otaian) pollen throughout the deposit [*Bannister et al.*, 2005; *Mildenhall et al.*, 2014] indicates that the maximum time span covered by the maar sediments is from the latest Oligocene to the early Miocene.

The precise timing and duration of the deposit cannot be established given the data presented here. However, the presence of laminated light/dark couplets strongly suggests annual deposition (biogenic/

lithogenic varves), which indicates a duration for the deposit of ~95,000 years. Laminated biogenic sediments do not always indicate annual deposition, however, with known deposits ranging from 0.3 laminae/yr to 2 laminae/yr [*Crusius and Anderson*, 1992], although annual deposition is by far the most common case [*Anderson*, 1986]. While a nonannual origin for the light/dark couplets in Foulden Maar cannot be ruled out, it seems likely that this deposit covers at least ~50,000 years, with initiation of lake sedimentation occurring some time in the latest Oligocene or the first 20,000 years of the Miocene. The combination of pollen dating [*Mildenhall et al*., 2014] and radiometric dating places deposition of the sequence within the period of rapid glaciation and subsequent deglaciation of Antarctica known as the Mi-1 event, which lasted from ~23.3 to 22.9 Ma [e.g., *Miller et al*., 1991; *Zachos et al*., 2001; *Wilson et al*., 2008].

5.2. Magnetic Mineralogy of the Foulden Maar Diatomite

The combination of high proportions of diamagnetic minerals and low proportions of ferrimagnetic minerals in the Foulden Maar diatomite creates a challenge for investigating magnetic mineralogy. In-field measurements provide little useful data. None of the measurements and comparisons discussed above are sufficient on their own to characterize the magnetic mineralogy of the Foulden Maar diatomite. In combination, however, and taking into account limited SEM observations, they allow us to draw the following conclusions.

1. AF demagnetization of ARM is consistent with the presence of either magnetite or pyrrhotite and rules out greigite.
2. Acquisition, AF demagnetization, and backfield demagnetization of IRM are consistent with the presence of pyrrhotite in the PSD to SD size range.
3. Values of IRM parameters are consistent with the presence of pyrrhotite or titanomagnetite; if pyrrhotite is assumed, a comparison with published parameters for sized fractions of pyrrhotite indicates a PSD grain-size range of 3–10 μm.
4. IRM unmixing was inconclusive due to the noisy nature of the data, but may indicate two populations of pyrrhotite grains with slightly different coercivity characteristics.
5. Micron-sized monoclinic and hexagonal pyrrhotite were observed using SEM.

Results for all measurements combine to indicate a relatively uniform magnetic mineral assemblage in which the primary remanence carrier is a population of PSD-sized pyrrhotite grains, with variable concentration with depth and facies. This is consistent with SEM observations of micron-sized pyrrhotite grains.

The complete lack of bioturbation and high organic content of the core suggest continual anoxia during deposition of the lake sediments. The hematite indicated in the sediments below 50 m is therefore relatively unlikely to be primary, since iron oxides are unstable in anoxic environments, and hematite tends to transform into pyrite [*Berner*, 1981]. The hematite may be associated with partial oxidation of pyrrhotite and pyrite in the period since core retrieval. This hypothesis is consistent with the observation of red coatings on core sections from deeper in the deposit during sampling.

The presence of pyrrhotite in the schist in the immediate vicinity of the maar at the time of crater formation is indicated by the thermal demagnetization of a three-component IRM from schist samples and identification of pyrrhotite grains under SEM in one schist sample. The damaged, fragmentary nature of the pyrrhotite grains observed in the sediment suggest a detrital origin. Furthermore, the presence of similarly damaged—and thus likely detrital—native copper grains in the sediment suggests an erosional link with the schist, which is known to contain copper-bearing veins [*Coombs et al*., 1993]. Although authigenesis is often cited as an origin for sedimentary pyrrhotite [e.g., *Roberts and Turner*, 1993], *Horng and Roberts* [2006] demonstrated that detrital pyrrhotite can exist in sedimentary environments when rapid source-to-sink transportation has occurred, and that it may be much more common than previously appreciated. The increased remanence of turbidite beds compared to laminated sections is also consistent with a detrital phase as the main magnetic carrier, as turbidite beds have a higher concentration of terrigenous material.

Authigenic pyrrhotite is most frequently found where tectonic deformation events or sulfide fluid/gas circulation have occurred [e.g., *Urbat et al*., 2000; *Weaver et al*., 2002; *Larrasoaña et al*., 2007; *Roberts et al*., 2010]. No such tectonic events are evident in the sedimentary record at Foulden Maar [*Jones*, 2011]. Significant long-lasting hydrothermal activity is also not usual in monogenetic volcanic settings [e.g., *Bahadori et al*.,

2013]. With the exception of localities affected by tectonic or hydrothermal events, authigenic pyrrhotite has only been reported to date in one lacustrine deposit, which was deposited under unusually saline and alkaline conditions [*Tuttle and Goldhaber*, 1993]. The high rainfall associated with the youngest lake sediments at Foulden Maar [*Reichgelt et al*., 2013] combined with the depth of the maar crater and the lack of evaporitic deposits make it highly unlikely that this lake was saline. Therefore, we conclude that the dominant magnetic carrier in the sediment is PSD-sized detrital pyrrhotite derived from the surrounding country rock.

5.3. Environmental Interpretation

The Foulden Maar diatomite can be divided into two depth zones on the basis of κ and ARM values, which are here taken as a proxy for magnetic mineral concentration. Zone A (39–102 mcd) has high to intermediate ARM and κ values and variance. Thin intervals with higher κ and ARM are superimposed on an overall decreasing trend (Figure 10). Zone B (6–39 mcd) has low overall κ and ARM and low variance.

Maar volcanoes in hard-rock environments such as the Otago Schist are usually characterized by a tephra ring, formed during the eruption, which contains large quantities of clasts from the surrounding country rock [*Lorenz*, 2003]. Although this tephra ring has been eroded away in the case of Foulden Maar, it seems probable that a large proportion of the allochthonous material—and thus the pyrrhotite—found within the diatomite was eroded from this volcaniclastic deposit, rather than from the hard crystalline schist itself.

Pyrrhotite, like other iron sulfides, is easily oxidized when it comes into contact with the atmosphere or oxic water, as shown by the partial oxidation of pyrrhotite grains in the sediment core after only a few years' exposure to oxygen. For detrital pyrrhotite from the original maar-forming eruption to have been preserved in the Foulden Maar diatomite, it must have passed through three stages: (1) deposition and preservation in an anoxic environment immediately after the eruption, (2) rapid erosion and transportation to the lake floor at some point after the eruption, and (3) redeposition in an anoxic environment on the lake floor.

Experiments on pyrrhotite-rich mine-tailings have found that pyrrhotite is well preserved in water-saturated sediments below about 1 m depth [*Gunsinger et al*., 2006]. This offers a model for preserving detrital pyrrhotite in the tephra ring from the time of the maar-forming eruption to the time of erosion and redeposition in the lake (stage 1). Transportation of material from the tephra ring to the anoxic lake bottom must have been relatively rapid for pyrrhotite to have been preserved (stage 2). Long residence times in soils or the shallow margins of the lake would result in pyrrhotite depletion through exposure to oxic waters. Variations in the concentration of detrital pyrrhotite must therefore represent variations in erosion and transportation rates. The absence of bioturbation in the lake sediments suggests that the lake floor was at all times anoxic, which is ideal for pyrrhotite preservation (stage 3). Variations in pyrrhotite concentration are, therefore, unlikely to represent variations in preservation (level of anoxia) on the lake floor.

Following the above logic, we interpret increased detrital pyrrhotite concentrations in the laminated sediments as representing one or a combination of two factors: (1) high erosion rates of the tephra ring and/or (2) rapid transportation from the tephra ring to the lake floor. These conditions are likely to have prevailed in the first few hundreds of years of maar history, while recolonization by vegetation was still under way and the maar sides were still being stabilized by mass flow deposits (for discussion of the development of maar systems, see *Pirrung et al*. [2003] and *White and Ross* [2011]). However, Zone A, which includes ~60,000 light/dark couplets, most likely represents a depositional period of several tens of thousands of years, a much greater span of time than is generally required for maar stabilization. Thus, a different explanation must be sought for the decreasing κ and ARM trends in this zone.

Couplet thickness in the core is broadly inversely proportional to ARM and κ, with an increasing trend upcore and low values in intervals of DLDA. Since couplet thickness variation is largely determined by the thickness of the light layers, which represent diatom blooms, couplet thickness variation can be taken as a measure of diatom productivity. The increase in couplet thickness upcore must be at least partly due to compaction; however, this cannot explain the reduced couplet thickness seen in DLDA intervals.

A number of factors can affect diatom productivity, including water temperature, windiness and nutrient cycling. However, studies of Quaternary diatom-dominated lakes have found that climate is the dominant control on productivity, although the exact mechanisms are not always known [*Williams et al*., 1997]. Variations in erosional input are also likely to be due directly or indirectly to climatic or environmental changes,

such as variation in vegetation cover on the crater rim or changes in precipitation. The anticovariance between κ and ARM on the one hand and couplet thickness on the other, at least in the DLDA intervals and possibly also across the entire length of the core, suggests that the two sets of proxies may be responding to a single set of environmental forcing factors. The decrease in ARM and κ upcore thus indicates that a long-term environmental change occurred at the site during the latest Oligocene/earliest Miocene. This long-term change may have been coeval with the Mi-1 event. However, further dating work is required to determine the length of the record represented by the deposit and the precise relationship with Mi-1.

6. Conclusions

The $^{40}Ar/^{39}Ar$ date of 23.38 $\pm$ 0.24 Ma obtained from basalt clast sample V14 is consistent with both the previously obtained date of 23.17 $\pm$ 0.19 Ma [*Lindqvist and Lee*, 2009] and the Early Miocene pollen found at the top of the studied deposit. The greater degree of alteration observed in basalt clast V15 suggests that of the two, V14 should be considered more reliable. Combined $^{40}Ar/^{39}Ar$, lamina counting and pollen ages indicate that the lake sediments were deposited over at least several tens of thousands of years during the latest Oligocene/earliest Miocene, and may have coincided with the period of rapid glaciation and subsequent deglaciation of Antarctica known as the Mi-1 event (peak at 23.03 Ma).

The primary carrier of the magnetic signal in the Foulden Maar diatomite is an assemblage of PSD pyrrhotite grains. This assemblage is detrital in origin, and is interpreted to have derived from the schist country rock surrounding the maar, probably by way of a now-eroded tephra ring. Pyrrhotite concentration varies with time and facies, but it is relatively uniform in composition and grain size throughout the $\sim$100 m thick succession. The presence of detrital pyrrhotite supports the claim by *Horng and Roberts* [2006] that detrital pyrrhotite may be a more common carrier of primary remanence in sedimentary environments than has previously been assumed.

Variations in pyrrhotite concentration in Foulden Maar reflect an initially mechanically unstable environment immediately following maar formation. This phase was followed by a longer period of gradually increasing stability, punctuated by short periods of relatively high erosion. The final depositional phase was characterized by stable conditions, with low erosional input. This decrease in erosional input suggests that a long-term (tens of thousands of years) climatic change occurred in New Zealand in the latest Oligocene/earliest Miocene, and may reflect broader changes associated with the Mi-1 event.

Acknowledgments
This research was funded by the Marsden Fund of the Royal Society of New Zealand. Bethany Fox was supported by a postgraduate scholarship from the University of Otago. The authors thank Webster Drilling for conducting the drilling operations, Featherston Resources and the Gibson and McRae families for access to the site, and Daniel Jones, Andy Clifford, and Bob Dagg for their assistance. Many thanks to the Editor and to Andrew Roberts, Massimo Mattei, and three anonymous reviewers for their constructive and helpful comments on the manuscript. The data used to produce the results in the paper are archived at www.pangaea.de, doi 10.1594/PANGAEA.834782.

References

Adams, C. J., and P. Robinson (1993), Potassium–argon age studies of metamorphism/uplift/cooling in Haast Schist coastal sections south of Dunedin, Otago, New Zealand, *N. Z. J. Geol. Geophys.*, *36*, 317–325.
Anderson, R. Y. (1986), The varve microcosm: Propagator of cyclic bedding, *Paleoceanography*, *1*, 373–382.
Bahadori, A., S. Zendehboudi, and G. Zahedi (2013), A review of geothermal energy resources in Australia: Current status and prospects, *Renewable Sustainable Energy Rev.*, *21*, 29–34.
Bannister, J. M., D. E. Lee, and J. I. Raine (2005), Morphology and palaeoenvironmental context of *Fouldenia staminosa*, a fossil flower with associated pollen from the Early Miocene of Otago, New Zealand, *N. Z. J. Bot.*, *43*, 515–525.
Berner, R. A. (1981), A new geochemical classification of sedimentary environments, *J. Sediment. Petrol.*, *51*, 359–365.
Blanchet, C. L., N. Thouveny, and L. Vidal (2009), Formation and preservation of greigite (Fe_3S_4) in sediments from the Santa Barbara Basin: Implications for paleoenvironmental change during the past 35 ka, *Paleoceanography*, *24*, PA2224, doi:10.1029/2008PA001719.
Canfield, D. E., and R. A. Berner (1987), Dissolution and pyritization of magnetite in anoxic marine sediments, *Geochim. Cosmochim. Acta*, *51*, 645–659.
Clark, D. A. (1984), Hysteresis properties of sized dispersed monoclinic pyrrhotite grains, *Geophys. Res. Lett.*, *11*, 173–176.
Coombs, D. S., Y. Kawachi, and A. Reay (1993), An occurrence of Ardennite in quartz veins in piemontite schist, Western Otago, New Zealand, *Mineral. Petrol.*, *48*, 295–308.
Coombs, D. S., C. J. Adams, B. P. Roser, and A. Reay (2008), Geochronology and geochemistry of the Dunedin Volcanic Group, eastern Otago, New Zealand, *N. Z. J. Geol. Geophys.*, *51*, 195–218.
Craw, D. (1984), Lithologic variations in Otago Schist, Mt Aspiring area, northwest Otago, New Zealand, *N. Z. J. Geol. Geophys.*, *27*, 151–166.
Crusius, J., and R. F. Anderson (1992), Inconsistencies in accumulation rates of Black Sea sediments inferred from records of laminae and ^{210}Pb, *Paleoceanography*, *7*, 215–227.
Dekkers, M. J. (1988), Magnetic properties of natural pyrrhotite part I: Behaviour of initial susceptibility and saturation-magnetization-related rock-magnetic parameters in a grain-size dependent framework, *Phys. Earth Planet. Inter.*, *52*, 376–393.
Egli, R. (2003), Analysis of the field dependence of remanent magnetization curves, *J. Geophys. Res.*, *108*(B2), 2081, doi:10.1029/2002JB002023.
Evans, M. E., and F. Heller (2003), *Environmental Magnetism: Principles and Applications of Enviromagnetics*, Academic, Amsterdam.
Forsyth, P. J. (2001), *Geology of the Waitaki Area*, Inst. of Geol. and Nucl. Sci., Lower Hutt, New Zealand.
Graham, I. J., and N. Mortimer (1992), Terrane characterisation and timing of metamorphism in the Otago Schist, New Zealand, using Rb–Sr and K–Ar geochronology, *N. Z. J. Geol. Geophys.*, *35*, 391–401.

Gunsinger, M. R., C. J. Ptacek, D. W. Blowes, and J. L. Jambor (2006), Evaluation of long-term sulfide oxidation processes within pyrrhotite-rich tailings, Lynn Lake, Manitoba, *J. Contam. Hydrol.*, *83*, 149–170.

Hay, R., and D. Craw (1993), Syn-metamorphic gold mineralisation, Invincible Vein, NW Otago Schist, New Zealand, *Mineral. Deposita*, *28*, 90–98.

Heslop, D., and M. Dillon (2007), Unmixing magnetic remanence curves without *a priori* knowledge, *Geophys. J. Int.*, *170*, 556–566.

Heslop, D., M. Dekkers, P. Kruiver, and I. van Oorschot (2001), *IRMunmix V2.2 Manual*.

Heslop, D., M. J. Dekkers, P. P. Kruiver, and I. H. M. van Oorschot (2002), Analysis of isothermal remanent magnetization acquisition curves using the expectation–maximization algorithm, *Geophys. J. Int.*, *148*, 58–64.

Hoernle, K., J. D. L. White, P. van den Bogaard, F. Hauff, D. S. Coombs, R. Werner, C. Timm, D. G.-S. Berg, A. Reay, and A. F. Cooper (2006), Cenozoic intraplate volcanism on New Zealand: Upwelling induced by lithospheric removal, *Earth Planet. Sci. Lett.*, *248*, 350–367.

Horng, C.-S., and A. P. Roberts (2006), Authigenic or detrital origin of pyrrhotite in sediments? Resolving a paleomagnetic conundrum, *Earth Planet. Sci. Lett.*, *241*, 750–762.

Jiang, W.-T., C.-S. Horng, A. P. Roberts, and D. R. Peacor (2001), Contradictory magnetic polarities in sediments and variable timing of neoformation of authigenic greigite, *Earth Planet. Sci. Lett.*, *193*, 1–12.

Jones, D. (2011), The geophysical characterisation of Foulden Maar, MS thesis, Dep. of Geol., Univ. of Otago, Dunedin, New Zealand.

Kruiver, P. P., M. J. Dekkers, and D. Heslop (2001), Quantification of magnetic coercivity components by the analysis of acquisition curves of isothermal remanent magnetisation, *Earth Planet. Sci. Lett.*, *189*, 269–276.

Larrasoaña, J. C., A. P. Roberts, R. J. Musgrave, E. Gràcia, E. Piñero, M. Vega, and F. Martínez-Ruiz (2007), Diagenetic formation of greigite and pyrrhotite in gas hydrate marine sedimentary systems, *Earth Planet. Sci. Lett.*, *261*, 350–366.

LeMasurier, W. E., and C. A. Landis (1996), Mantle-plume activity recorded by low-relief erosion surfaces in West Antarctica and New Zealand, *Geol. Soc. Am. Bull.*, *108*, 1450–1466.

Lindqvist, J. K., and D. E. Lee (2009), High-frequency paleoclimate signals from Foulden Maar, Waipiata Volcanic Field, southern New Zealand: An Early Miocene varved lacustrine diatomite deposit, *Sediment. Geol.*, *222*, 98–110, doi:10.1016/j.sedgeo.2009.07.009.

Liu, Q., A. P. Roberts, J. C. Larrasoaña, S. K. Banerjee, Y. Guyodo, L. Tauxe, and F. Oldfield (2012), Environmental magnetism: Principles and applications, *Rev. Geophys.*, *50*, RG4002, doi:10.1029/2012RG000393.

Lorenz, V. (2003), Maar-diatreme volcanoes, their formation, and their setting in hard-rock or soft-rock environments, *GeoLines*, *15*, 72–83.

Lowrie, W. (1990), Identification of ferromagnetic minerals in a rock by coercivity and unblocking temperature properties, *Geophys. Res. Lett.*, *17*, 159–162.

Lurcock, P. (2012), Palaeomagnetism of Palaeogene strata from Southern Zealandia: Implications for ice in the greenhouse, PhD thesis, Dep. of Geol., Univ. of Otago, Dunedin, New Zealand.

Mildenhall, D. C., E. M. Kennedy, D. E. Lee, U. Kaulfuss, J. M. Bannister, B. Fox, and J. G. Conran (2014), Palynology of the early Miocene Foulden Maar, Otago, New Zealand: Diversity following destruction, *Rev. Palaeobot. Palynol.*, *204*, 27–42.

Miller, K. G., J. D. Wright, and R. G. Fairbanks (1991), Unlocking the ice house—Oligocene–Miocene oxygen isotopes, eustasy, and margin erosion, *J. Geophys. Res.*, *96*, 6829–6848.

Németh, K. (2001), Phreatomagmatic volcanism at the Waipiata Volcanic Field, Otago, New Zealand, PhD thesis, Dep. of Geol., Univ. of Otago, Dunedin, New Zealand.

Peters, C., and M. J. Dekkers (2003), Selected room temperature magnetic parameters as a function of mineralogy, concentration and grain size, *Phys. Chem. Earth*, *28*, 659–667, doi:10.1016/S1474-7065(03)00120-7.

Peters, C., and R. Thompson (1998), Magnetic identification of selected natural iron oxides and sulphides, *J. Magn. Magn. Mater.*, *183*, 365–374.

Pirrung, M., C. Fischer, G. Buchel, R. Gaupp, H. Lutz, and F.-O. Neuffer (2003), Lithofacies succession of maar crater deposits in the Eifel area (Germany), *Terra Nova*, *15*, 125–132.

Reichgelt, T., E. M. Kennedy, D. C. Mildenhall, J. G. Conran, D. R. Greenwood, and D. E. Lee (2013), Quantitative palaeoclimate estimates for Early Miocene southern New Zealand: Evidence from Foulden Maar, *Palaeogeogr. Palaeoclimatol. Palaeoecol.*, *378*, 36–44.

Reynolds, R. L., J. G. Rosenbaum, P. van Metre, M. Tuttle, E. Callender, and A. Goldin (1999), Greigite (Fe_3S_4) as an indicator of drought—The 1912–1994 sediment magnetic record from White Rock Lake, Dallas, Texas, USA, *J. Paleolimnol.*, *21*, 193–206.

Roberts, A. P., and G. M. Turner (1993), Diagenetic formation of ferrimagnetic iron sulphide minerals in rapidly deposited marine sediments, South Island, New Zealand, *Earth Planet. Sci. Lett.*, *115*, 257–273.

Roberts, A. P., F. Florindo, J. C. Larrasoaña, M. A. O'Regan, and X. Zhao (2010), Complex polarity pattern at the former Plio-Pleistocene global stratotype section at Vrica (Italy): Remagnetization by magnetic iron sulphides, *Earth Planet. Sci. Lett.*, *292*, 98–111.

Roberts, A. P., L. Chang, C. J. Rowan, C.-S. Horng, and F. Florindo (2011), Magnetic properties of sedimentary greigite (Fe_3S_4): An update, *Rev. Geophys.*, *49*, RG1002, doi:10.1029/2010RG000336.

Robertson, D. J., and D. E. France (1994), Discrimination of remanence-carrying minerals in mixtures, using isothermal remanent magnetisation acquisition curves, *Phys. Earth Planet. Inter.*, *82*, 223–234.

Snowball, I., and M. Torii (1999), Incidence and significance of magnetic iron sulphides in Quaternary sediments and soils, in *Quaternary Climates, Environments and Magnetism*, edited by B. A. Maher and R. Thompson, pp. 199–230, Cambridge Univ. Press, Cambridge, U. K.

Steiger, R. H., and E. Jäger (1977), Subcommission of geochronology: Convention on the use of decay constants in geo- and cosmochronology, *Earth Planet. Sci. Lett.*, *36*, 359–362.

Sutherland, R. (1995), The Australia–Pacific boundary and Cenozoic plate motions in the SW Pacific: Some constraints from Geosat data, *Tectonics*, *14*, 819–831.

Symons, D. T. A., and M. T. Cioppa (2000), Crossover plots: A useful method for plotting SIRM data in paleomagnetism, *Geophys. Res. Lett.*, *27*, 1779–1782.

Thompson, R., and F. Oldfield (1986), *Environmental Magnetism*, Allen and Unwin, London.

Torii, M., K. Fukuma, C.-S. Horng, and T.-Q. Lee (1996), Magnetic discrimination of pyrrhotite- and greigite-bearing sediment samples, *Geophys. Res. Lett.*, *23*, 1813–1816.

Turrin, B. D., J. M. Donnelly-Nolan, and B. C. Hearn (1994), $^{40}Ar/^{39}Ar$ ages from the rhyolite of Alder Creek, California: Age of the Cobb Mountain normal-polarity subchron revisited, *Geology*, *22*, 251–254.

Turrin, B. D., R. L. Christiansen, M. A. Clynne, D. E. Champion, W. J. Gerstel, L. J. Muffler, and D. A. Trimble (1998), The age of Lassen Peak, California, a young heterogeneous dacite dome, and implication for the ages of Late Pleistocene glaciations in the Southern Cascade Range, *Geol. Soc. Am. Bull.*, *110*, 931–945.

Turrin, B. D., J. T. Gutmann, and C. C. Swisher III (2008), A 13 ± 3 ka age determination of a tholeiite, Pinacate volcanic field, Mexico, and improved methods for $^{40}Ar/^{39}Ar$ dating of young basaltic rocks, *J. Volcanol. Geotherm. Res.*, *177*, 848–856.

Turrin, B. D., C. C. Swisher III, and A. L. Deino (2010), Mass discrimination monitoring and inter-calibration of dual collectors in noble-gas mass spectrometer systems, *Geochem. Geophys. Geosyst.*, *11*, Q0AA09, doi:10.1029/2009GC003013.

Tuttle, M. L., and M. B. Goldhaber (1993), Sedimentary sulfur geochemistry of the Paleogene Green River Formation, western USA: Implications for interpreting depositional and diagenetic processes in saline alkaline lakes, *Geochim. Cosmochim. Acta*, *57*, 3023–3039.

Urbat, M., M. J. Dekkers, and K. Krumsiek (2000), Discharge of hydrothermal fluids through sediment at the Escanaba Trough, Gorda Ridge (ODP Leg 169): Assessing the effects on the rock magnetic signal, *Earth Planet. Sci. Lett.*, *176*, 481–494.

Vaughan, D. J., E. J. Schwarz, and D. R. Owens (1971), Pyrrhotites from the Strathcoma mine, Sudbury, Canada: A thermomagnetic and mineralogical study, *Econ. Geol.*, *66*, 1131–1144.

Weaver, R., A. P. Roberts, and A. J. Barker (2002), A late diagenetic (syn-folding) magnetization carried by pyrrhotite: Implications for paleomagnetic studies from magnetic iron sulphide-bearing sediments, *Earth Planet. Sci. Lett.*, *200*, 371–386.

Weeks, R., C. Laj, L. Endignoux, M. Fuller, A. Roberts, R. Manganne, E. Blanchard, and W. Goree (1993), Improvements in long-core measurement techniques: Applications in palaeomagnetism and palaeoceanography, *Geophys. J. Int.*, *114*, 651–662.

White, J. D. L., and P.-S. Ross (2011), Maar-diatreme volcanoes: A review, *J. Volcanol. Geotherm. Res.*, *201*, 1–29.

Wilkin, R. T., and H. L. Barnes (1996), Pyrite formation by reactions of iron monosulfides with dissolved inorganic and organic sulfur species, *Geochim. Cosmochim. Acta*, *60*, 4167–4179.

Williams, D. F., J. Peck, E. B. Karabanov, A. A. Prokopenko, V. Kravchinsky, J. King, and M. I. Kuzmin (1997), Lake Baikal record of continental climate response to orbital insolation during the past 5 million years, *Science*, *278*, 1114–1117.

Wilson, G. S., S. F. Pekar, T. R. Naish, S. Passchier, and R. DeConto (2008), The Oligocene-Miocene boundary—Antarctic climate response to orbital forcing, in *Antarctic Climate Evolution, Developments in Earth and Environmental Sciences*, vol. 8, edited by F. Florindo and M. Siegert, pp. 369–399, Elsevier, Amsterdam. doi:10.1016/S1571-9197(08)00009-8.

Zachos, J. C., N. J. Shackleton, J. S. Revenaugh, H. Pälike, and B. P. Flower (2001), Climate response to orbital forcing across the Oligocene–Miocene boundary, *Science*, *292*, 274–278.